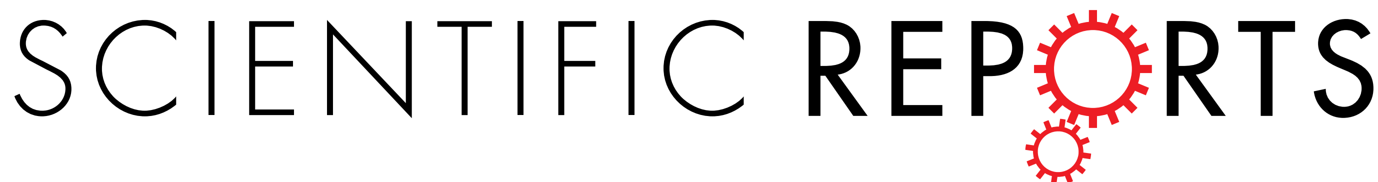

OPEN

# Growth of vanadium dioxide thin films on hexagonal boron nitride flakes as transferrable substrates

Received: 15 October 2018
Accepted: 16 January 2019
Published online: 27 February 2019

Shingo Genchi[1], Mahito Yamamoto[1], Koji Shigematsu[2], Shodai Aritomi[3], Ryo Nouchi[4,5], Teruo Kanki[1], Kenji Watanabe[6], Takashi Taniguchi[6], Yasukazu Murakami[2,3] & Hidekazu Tanaka[1]

**Vanadium dioxide ($VO_2$) is an archetypal metal-insulator transition (MIT) material, which has been known for decades to show an orders-of-magnitude change in resistivity across the critical temperature of approximately 340 K. In recent years, $VO_2$ has attracted increasing interest for electronic and photonic applications, along with advancement in thin film growth techniques. Previously, thin films of $VO_2$ were commonly grown on rigid substrates such as crystalline oxides and bulk semiconductors, but the use of transferrable materials as the growth substrates can provide versatility in applications, including transparent and flexible devices. Here, we employ single-crystalline hexagonal boron nitride (hBN), which is an insulating layered material, as a substrate for $VO_2$ thin film growth. $VO_2$ thin films in the polycrystalline form are grown onto hBN thin flakes exfoliated onto silicon (Si) with a thermal oxide, with grains reaching up-to a micrometer in size. The $VO_2$ grains on hBN are orientated preferentially with the (110) surface of the rutile structure, which is the most energetically favorable. The $VO_2$ film on hBN shows a MIT at approximately 340 K, across which the resistivity changes by nearly three orders of magnitude, comparable to $VO_2$ films grown on common substrates such as sapphire and titanium dioxide. The $VO_2$/hBN stack can be picked up from the supporting Si and transferred onto arbitrary substrates, onto which $VO_2$ thin films cannot be grown directly. Our results pave the way for new possibilities for practical and versatile applications of $VO_2$ thin films in electronics and photonics.**

In recent decades, transition metal oxides that undergo metal-insulator transitions (MITs) have attracted much attention as components for electronic and photonic devices. In particular, vanadium dioxide ($VO_2$) has been of great interest for practical applications because the MIT for $VO_2$ is induced near room temperature (~340 K)[1]. Additionally, the MIT leads to dramatic changes in the electrical resistivity (up-to five orders of magnitude in a single crystal)[2] as well as optical transmittance (more than 50% in the infrared range)[3]. More importantly, thanks to advancements in thin film growth techniques, $VO_2$ can be prepared consistently in thin film form, with properties comparable to those of the bulk counterpart[4]. In fact, the growth of high-quality $VO_2$ thin films has been demonstrated even on the wafer scale, which is promising for practical use in electronics and photonics[5].

Commonly, thin films of $VO_2$ have been prepared on oxide substrates because a high-temperature oxygen ($O_2$) treatment is often necessary for crystallization. Some of the most common substrates include aluminum oxide ($Al_2O_3$)[6] and titanium dioxide ($TiO_2$)[7], on which $VO_2$ films show a MIT with resistivity changing by up-to four orders of magnitude. Additionally, non-oxide materials have been employed as substrates for $VO_2$ growth, such as silicon (Si)[8], germanium[9], and gallium nitride[10]. Even on such semiconducting compounds, $VO_2$ films show reasonable MIT properties, opening the possibility for the realization of electronic and photonic $VO_2$ devices compatible with existing semiconductor technology. On these rigid substrates, the fabrication of devices is, in principle, based on the top-down integration of other components onto $VO_2$. However, if $VO_2$ thin films can

[1]Institute of Scientific and Industrial Research, Osaka University, Ibaraki, Osaka, 567-0047, Japan. [2]The Ultramicroscopy Research Center, Kyushu University, Fukuoka, 819-0395, Japan. [3]Department of Applied Quantum Physics and Nuclear Engineering, Faculty of Engineering, Kyushu University, Fukuoka, 819-0395, Japan. [4]Graduate School of Engineering, Osaka Prefecture University, Sakai, Osaka, 599-8570, Japan. [5]JST PRESTO, Kawaguchi, Saitama, 332-0012, Japan. [6]National Institute for Materials Science, Tsukuba, Ibaraki, 305-0044, Japan. Correspondence and requests for materials should be addressed to M.Y. (email: mahito.yamamoto@sanken.osaka-u.ac.jp) or H.T. (email: h-tanaka@sanken.osaka-u.ac.jp)

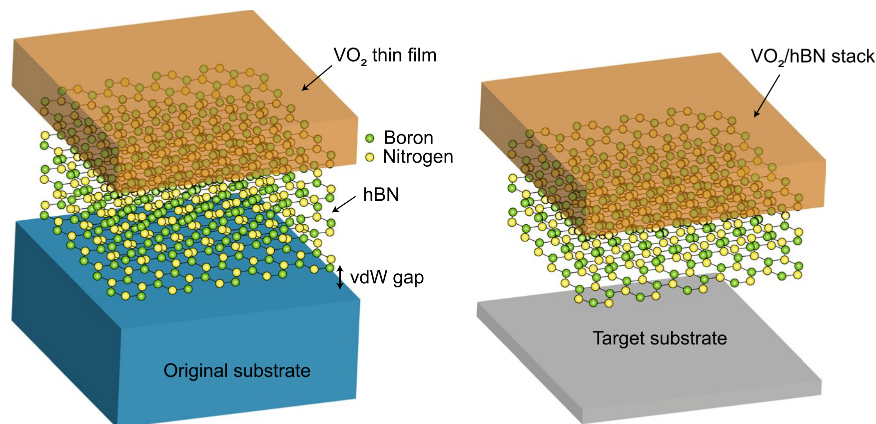


**Figure 1.** Schematic illustration of the growth of the $VO_2$ thin film on a hBN flake supported on a substrate (left). Due to the weak van der Waals (vdW) interaction between hBN and the substrate, the stack of $VO_2$ and hBN is expected to be transferred from the original substrate onto a target substrate of any material and geometry (right).

be prepared on thin transferable supports, the range of device applications is expected to be extended further, including for example, flexible devices.

Recently, with the progress of research on two-dimensional (2D) layered materials, layered materials have attracted interest as transferable substrates for growth of $VO_2$ thin films. Recent studies have reported that $VO_2$ thin films can be grown on chemical vapor deposited graphene on copper and that a $VO_2$/graphene stack can be transferred onto a plastic film for use in flexible thermochromic windows[11,12]. Additionally, growth of $VO_2$ on muscovite has been reported[13,14]. Thin films of muscovite could be peeled off from the bulk with the covering $VO_2$[14], hence promising flexible device applications. Although these results suggest the utility of layered materials for the $VO_2$ growth substrate, their potential applications may be limited in number because graphene shows an extremely high electrical conductivity, while muscovite is mechanically relatively fragile. Therefore, the search for alternative layered materials with insulating properties as well as mechanical strength is necessary for realizing more versatile applications.

Here, we demonstrate the growth of $VO_2$ thin films on crystalline hexagonal boron nitride (hBN), which is a layered material consisting of honeycomb lattices with nitrogen and boron atoms arranged at the inequivalent triangular sites. Hexagonal BN is electrically insulating even at nanometer thicknesses[15,16], due to a wide bandgap energy close to 6 eV[17,18]. Ultrathin hBN has a large Young's modulus of ~0.86 TPa and a fracture strength of ~70 GPa[19], comparable to those of diamond. In addition to these exceptional electronic and mechanical properties, hBN is inert to $O_2$ exposure even at 500 °C[20,21], making it a promising choice for use as an oxide growth substrate. We observed that $VO_2$ thin films could be grown on hBN with crystallinity and that such films underwent a MIT at approximately 340 K. Across the MIT, the resistivity was observed to change by nearly three orders of magnitude, which is comparable to that found for $VO_2$ thin films grown on common substrates[6–10]. More importantly, we found that the stack of $VO_2$ and hBN could be picked up from an original substrate, and, then, transferred onto another target substrate of any material and geometry, as schematically depicted in Fig. 1. These results have important implications for the realization of a variety of electronic and photonic devices based on $VO_2$/hBN stacks.

## Results and Discussion

For the $VO_2$ growth substrates, we used thin flakes of high-purity hBN single crystals, which were synthesized by the method described in ref.[22]. Using adhesive tape, thin flakes of hBN were mechanically exfoliated from bulk single crystals onto Si substrates with 285 nm-thick silicon dioxide ($SiO_2$) layers, leading to the (0001) surface facing upward. The exfoliated hBN flakes have atomically flat surfaces with few defects[15,16]. Following an $O_2$ treatment at 500 °C in ambient pressure for 3.5 hours to remove the adhesive tape residue[20], thin films of $VO_2$ were grown onto hBN by pulsed laser deposition (PLD, see Methods for more details). Figure 2a is a typical optical image of the hBN flakes supported on $SiO_2$/Si after the growth of a $VO_2$ thin film. The lateral sizes of the hBN flakes exfoliated on $SiO_2$ range up-to hundreds of micrometers in length. By measuring the height difference between the region covered with $VO_2$ and the substrate by using atomic force microscopy (AFM), the thickness of the deposited film was determined to be ~26.9 nm. Below, by using cross-sectional scanning transmission electron microscopy (STEM), we find that the thicknesses of films supported on $SiO_2$ and hBN are comparable to each other. First, the crystallinity of $VO_2$ on hBN was characterized using Raman spectroscopy. Figure 2b is a Raman spectrum obtained for $VO_2$ grown on a 226 nm-thick hBN flake at 300 K (see the inset for the optical image of the $VO_2$/hBN stack). In addition to the peaks for Si and hBN at 520 and 1367 $cm^{-1}$ [23,24], prominent Raman peaks from the vibration modes of monoclinic $VO_2$ were observed at 192, 222, 307, 389, and 614 $cm^{-1}$ [25], indicating the growth of the $VO_2$ crystal on hBN.

Additionally, we investigated the phase transition properties of the $VO_2$ films grown on hBN from temperature-dependent Raman spectroscopy measurements. As shown in Fig. 2c, the Raman peaks for $VO_2$ on a hBN flake were diminished above 340 K when heated up from 300 K but appeared when cooled down from 370 K

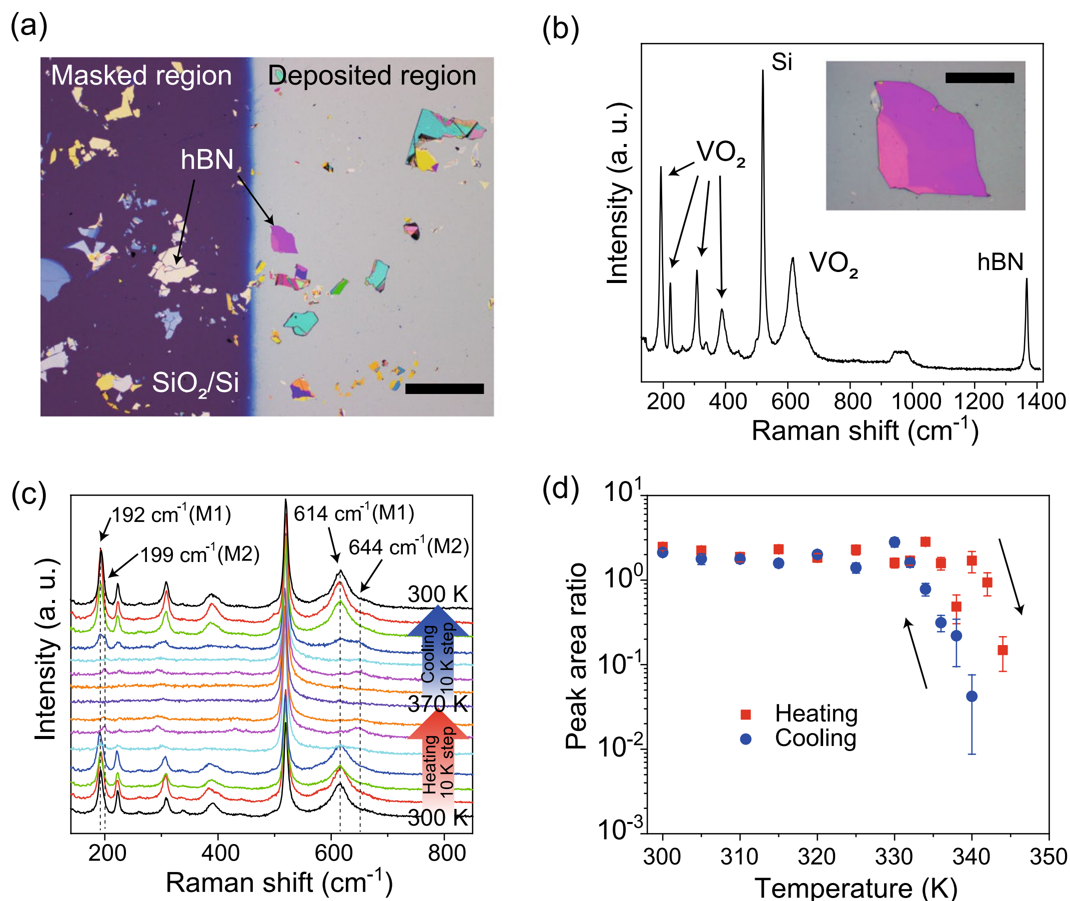


**Figure 2.** (**a**) Optical image of hBN flakes exfoliated onto a $SiO_2$/Si substrate after the growth of $VO_2$. The left purple region shows the $SiO_2$/Si surface, which was masked during the growth, while the deposited region is colored in gray. The scale bar is 250 µm. (**b**) Raman spectrum measured for the $VO_2$ thin film grown on hBN on $SiO_2$/Si at 300 K. The inset shows the optical image of the $VO_2$/hBN stack. The scale bar is 50 µm. (**c**) Temperature-dependent Raman spectra measured at $VO_2$ on hBN. The measurement temperature was increased from 300 to 370 K and, subsequently, decreased from 370 to 300 K with a 10 K step. (**d**) The area ratio of the $VO_2$ peak at 614 or 644 $cm^{-1}$ to the Si peak at 520 $cm^{-1}$ as a function of temperature in the heating (red square dot) and cooling (blue circular dot) processes.

below 330 K. The observations imply that $VO_2$ on hBN undergoes a structural phase transition between the monoclinic (which is commonly called the "M1" phase) and tetragonal structures at a temperature of approximately 340 K[26]. We note that the Raman peaks for $VO_2$ with a tetragonal structure are absent, as reported previously[25,26]. Noteworthy, near the transition temperature, strong peaks were observed at 199 and 644 $cm^{-1}$, rather than 192 and 614 $cm^{-1}$ (see Fig. 2c). The Raman peaks are characteristics of the monoclinic "M2" phase of $VO_2$, which is the metastable transient structure between the monoclinic M1 and tetragonal structures and can be stabilized by doping[27,28] or applying strain along the [110] direction of the rutile structure[29,30]. Although we cannot completely exclude the possibility of unintentional doping in $VO_2$ without a detailed chemical analysis, since no dopants were added during growth, the stabilization of the M2 phase in $VO_2$ on hBN is most likely due to strain along the [110] direction. Below, from cross-sectional STEM measurements, the $VO_2$ thin film is observed to be grown preferentially with the (110) orientation. Therefore, $VO_2$ is supposed to be compressively strained isotropically in the in-plane direction on hBN, leading to tensile strain along the [110] direction. Such interfacial strains have been observed in thin films grown on layered materials and are explained to be due to the dipole-dipole interactions[31]. Further detailed measurements with, for example, synchrotron X-ray diffraction spectroscopy will be needed to identify the cause of the stabilization of the M2 phase in $VO_2$ grown on hBN.

The transition temperature estimated from the Raman spectroscopy measurements in Fig. 2c is supposed to be lower than the exact transition temperature because the actual temperature of $VO_2$ is higher than the set value due to laser heating during the measurements. To further explore the critical temperature for the structural phase transition, we collected the Raman spectra for $VO_2$ using a much smaller laser intensity than that used in Fig. 2c (see Methods). Figure 2d shows the area ratio for the $VO_2$ peak at 614 or 644 $cm^{-1}$ to the Si peak at 520 $cm^{-1}$ as a function of temperature for the heating and cooling processes. We found that the Raman peak area ratio was reduced abruptly at 344 K in the heating process, but, in the cooling process, increased largely at 340 K. We note that the actual critical temperature for the structural phase transition of $VO_2$ could be still higher than the

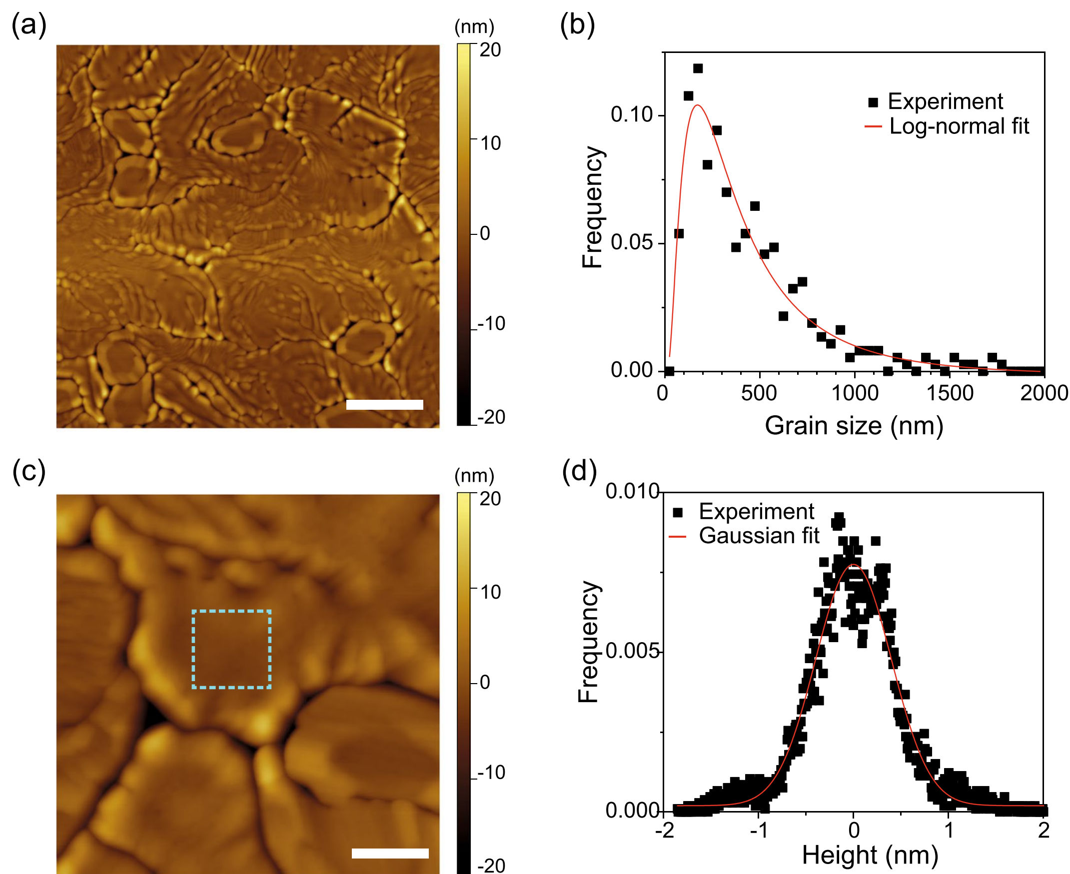


**Figure 3.** (**a**) AFM topographic image of $VO_2$ grown on hBN. The scale bar is 1 μm. (**b**) The distribution of the grain size of $VO_2$ (black square dots). The red curve is a logarithmic-normal fit. (**c**) Magnified AFM image of $VO_2$ on hBN. The scale bar is 200 nm. (**d**) The height histogram for the area surrounded by the dashed light blue line in (**c**). The red solid curve is a Gaussian fit with a standard deviation of 0.4 nm.

obtained values because the influence of laser heating cannot be completely ruled out. The observations suggest that the structural phase transition is induced with hysteresis. The magnitude of hysteresis is as small as that reported in the Raman spectroscopy measurement for single-crystalline $VO_2$[32], implying that the $VO_2$ film on hBN is a single crystal or polycrystalline with grain sizes comparable to the laser spot size of the Raman spectroscopy measurement of ~1 μm.

Next, we investigated the morphology of $VO_2$ thin films grown on hBN using AFM. Figure 3a shows an AFM image of a $VO_2$ thin film grown on a hBN flake collected at room temperature. The $VO_2$ thin film on hBN was observed to be composed of grains with meandering boundaries, thus suggesting a polycrystalline nature, at least, in the in-plane direction. To estimate the characteristic grain size of $VO_2$ on hBN, we measured the spacing between grain boundaries over the AFM image. Figure 3b shows the distribution of the $VO_2$ grain sizes on hBN. As often seen in polycrystalline films[33], the grain size distribution can be well fitted with a logarithmic-normal function, with the mean size determined to be 490 ± 60 nm in length. Although we cannot be certain that each grain is single-crystalline, the observed grain size as large as micrometers is consistent with the expectation from the Raman spectroscopy measurements. The grain size of $VO_2$ on hBN is one order of magnitude larger than that of polycrystalline $VO_2$ on $Al_2O_3(0001)$[34], where small grains are formed as a result of the ease of the large lattice mismatch strain (see Supplementary Information for the AFM image). Therefore, compared with the $VO_2$ films grown on $Al_2O_3$, $VO_2$ on hBN is supposed to be strained slightly during growth. While the grains of $VO_2$ on hBN were found to upheave by ~10 nm near the boundaries, which is likely due to the effect of grain boundary grooving[35], each grain has a relatively flat surface in the middle, with a roughness of $<0.4$ nm, as shown in the AFM image and the height distribution in Fig. 3c,d. The observation of an atomically flat surface may imply single crystallinity for each $VO_2$ grains on hBN.

To examine the crystallinity of the $VO_2$ grains on hBN at the atomic scale, we employed high-angle annular dark-field STEM (HAADF-STEM. See Methods for the details)[36]. The specimens for the STEM measurements were prepared by cutting a $VO_2$/hBN stack by focused ion beam milling. Figure 4a is a cross-sectional STEM image of the $VO_2$/hBN stack obtained at room temperature. While the crystal structure of hBN cannot be well resolved from this viewing angle, the lattice fringe is clearly seen for the $VO_2$ region over the sample. The inset in Fig. 4a shows the atomically resolved STEM image of hBN obtained from a different viewing angle. The darker regions imply that other $VO_2$ grains with different orientations are present along the projection direction in the specimen. The crystallinity of the $VO_2$ grain is confirmed from the sharp spots observed in the fast Fourier

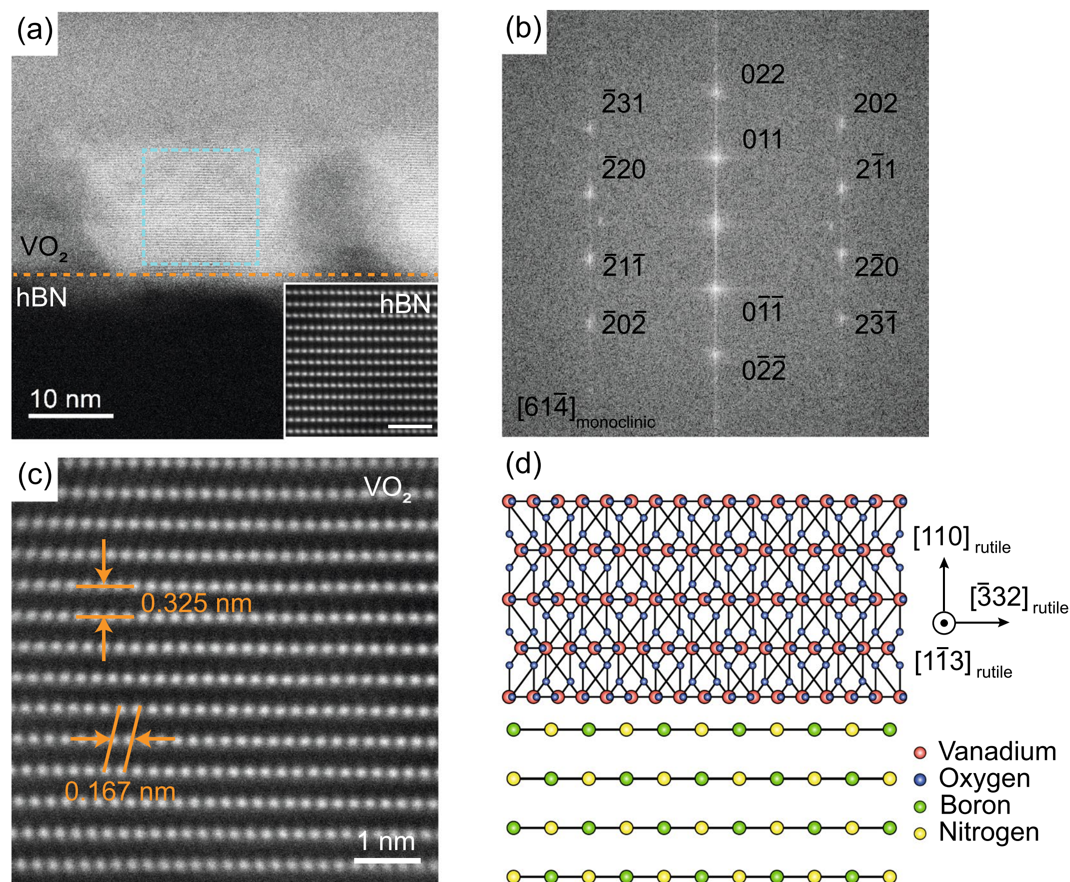


**Figure 4.** (**a**) Cross-sectional STEM image of the $VO_2$/hBN stack. The orange dashed line indicates the interface between $VO_2$ and hBN. The inset shows an atomically resolved STEM image of hBN. The scale bar in the inset is 1 nm. (**b**) FFT image of the $VO_2$ region surrounded by the dashed light blue line in (**a**). The Miller indices of the spots are indicated by choosing the $[61\bar{4}]$ of the monoclinic structure as the projection direction. (**c**) Atomically resolved STEM image of $VO_2$. (**d**) Schematic illustration of $VO_2$ grown on hBN with the orientation of the [110] direction of the rutile structure. The relative atomic position of $VO_2$ compared to hBN and the atomic structure of $VO_2$ at the interface do not necessary reflect the actual configuration.

transformation (FFT) image extracted from the area surrounded by the dashed light blue line in Fig. 4a (see Fig. 4b for the FFT image; the assignments for the spots will be discussed in the following). To determine the crystallographic orientation of the grain, we obtained a high-resolution STEM image of $VO_2$, as shown in Fig. 4c. Vanadium atoms are observed to be arranged with an out-of-plane spacing of 0.325 nm, with an in-plane spacing of 0.167 nm. We note that the out-of-plane lattice spacing of $VO_2$ is determined by calibration with a known interlayer spacing of hBN of 0.333 nm (see the inset of Fig. 4a). Since the monoclinic and rutile $VO_2$ show <1% difference in the spacing between neighboring vanadium atoms, we characterize the crystallographic orientation of the $VO_2$ grain based on the rutile structure, for simplicity. The out-of-plane lattice spacing of 0.325 nm could be assigned as the spacing between the (110) plane of the rutile $VO_2$, which is 0.322 nm for the bulk. Therefore, the $VO_2$ crystal on hBN is strained by 1% along the [110] direction of the rutile structure, while the in-plane strain is estimated to be 0.3% by assuming the Poisson's ratio to be 0.3[37]. Such magnitude of tensile strain along the [110] direction is large enough to stabilize the M2 phase in $VO_2$ near the transition temperature[29]. Given the observed in-plane spacing, the projection direction can be, therefore, identified along the $[1\bar{1}3]$ direction of the rutile structure (see Fig. 4d for a schematic illustration). In the presence of four crystallographic variants, there are four candidate directions in the monoclinic $VO_2$ (i.e., $[61\bar{2}]$, $[6\bar{1}\bar{2}]$, $[6\bar{1}\bar{4}]$, and $[61\bar{4}]$) to which the rutile $[1\bar{1}3]$ direction can be transformed. Therefore, among the variants taking the $[61\bar{4}]$ orientation for the projection, for example, the spots in the FFT image can be assigned, as shown in Fig. 4b.

From the STEM image of the other specimen, we observed that the $VO_2$ grain is, again, orientated along the [110] direction of the rutile structure (see Supplementary Information). Therefore, $VO_2$ is presumably grown on hBN, most preferentially with the (110) orientation of the rutile structure. We note that $VO_2$ is grown in the rutile structure since the growth temperature is 450 °C[4]. A density functional theory calculation has shown that the (110) surface is the most energetically favorable among the low Miller index planes of $VO_2$[38], and, indeed, growth of polycrystalline $VO_2$ films with the (110) orientation has been observed on Si and quartz[30]. Therefore, the preferential growth of the $VO_2$ film with the (110) orientation on hBN is legitimate because the hBN surface has no dangling bonds, and hence, only weak van der Waals interactions are expected to act at the interface (see Fig. 4d).

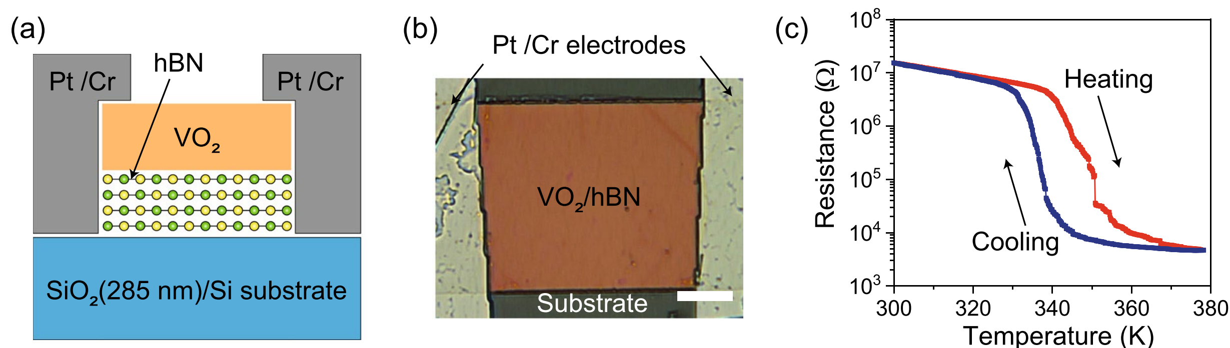


**Figure 5.** (**a**) Schematic and (**b**) optical images of the $VO_2$/hBN stack contacted with the Pt/Cr electrodes for the electrical measurements. The scale bar in the optical image is 10 μm. (**c**) Resistance-temperature characteristic of the $VO_2$/hBN stack. The electrical resistance of $VO_2$ was measured from 300 to 378 K (red curve) and, subsequently, from 378 to 300 K (blue curve).

Such so called "van der Waal epitaxy" of $VO_2$ has been reported previously on a muscovite(0001) substrate, but the growth orientation is not [110] but in the [010] direction[14]. This difference might be because the layers of muscovite are negatively charged[39] in contrast with hBN, and the electrostatic interactions, in addition to the van der Waals interactions, play a role at the growth interface. As shown in Supplementary Fig. S2, we also observed Moiré patterns in the STEM images of $VO_2$, which are most likely produced by superposition in the multiple grains and/or the monoclinic variants in the $VO_2$ film (see Fig. 3c for the AFM image of the $VO_2$ film with grains). To settle the growth orientations, therefore, further detailed analysis for the Moiré patterns as well as plan-view TEM measurements will be necessary.

From the Raman spectroscopy measurements, we found that $VO_2$ films grown on hBN underwent a structural phase transition at approximately 340 K (see Fig. 2d). Here, we investigate if the structural phase transition in $VO_2$ on hBN accompanies an electronic phase transition. Figure 5a,b show schematic and optical images of the $VO_2$/hBN stack with the platinum (Pt)/chromium (Cr) contact electrodes used for the electrical measurement. See Methods for details of the electrical measurements. The length and width of $VO_2$ between the electrodes was 41 and 37 μm, while the thickness of $VO_2$ and supporting hBN was estimated to be 40 and 90 nm, respectively. The resistance of $VO_2$ was measured in a two-probe configuration at temperatures ranging between 300 and 378 K. Figure 5c shows the resistance-temperature characteristics for $VO_2$ on hBN measured in the heating (red curve) and cooling (blue curve) processes. At 300 K, $VO_2$ shows a resistance of $<10^7$ Ω; however, the resistance was observed to be largely reduced with increasing temperature above ~344 K. Ultimately at 378 K, the resistance was decreased down to the order of $10^3$ Ω. Alternatively, when the $VO_2$ film was cooled down, the resistance showed a large increase below ~336 K. These observations clearly indicated that the MIT for $VO_2$ on hBN was thermally induced at approximately 340 K with hysteresis, similar to polycrystalline $VO_2$ films grown on other substrates such as $Al_2O_3$(0001)[6]. The magnitude of the resistance change across the MIT is comparable to that observed in $VO_2$ grown on common substrates[6–10], emphasizing the usefulness of hBN as the $VO_2$ growth substrate.

We observed several resistance jumps, particularly during the heating process for the resistance-temperature curve in Fig. 5c. Similar behaviors were previously observed for the resistance-temperature characteristics of $VO_2$ thin films grown on $Al_2O_3(10\bar{1}0)$[40] and $TiO_2$(001)[41], which were explained by the effects of the crystal domain sizes relative to the spacing between the measurement electrodes. Thin films of $VO_2$ commonly consist of crystal domains, with each domain having a slightly different critical temperature for the MIT. As a result, when the temperature-dependent electrical measurement is conducted for a $VO_2$ thin film, the resistance does not change thoroughly at a unique temperature, but gradually with temperature in a percolating manner. However, if the spacing between the measurement electrodes is narrowed down to the scale of the domain size, the formation of single percolation paths between the electrodes becomes marked in the resistance change, resulting in step-like behaviors in the resistance-temperature characteristics. The typical domain size for polycrystalline $VO_2$ on $Al_2O_3$ was measured to be tens of nanometers, and, hence, a nanometer-scale electrode spacing was necessary to observe such resistance jumps[40]. For single-crystalline $VO_2$ on $TiO_2$(001), the domain is regulated by the cracks formed in the film, which is as large as micrometers in size[41]. Therefore, resistance jumps were observed even for an electrode spacing of 50 μm. The resistance jumps in $VO_2$ on hBN were observed with a 41 μm-long electrode spacing, implying that the characteristic domain size is on the order of hundreds of nanometers or even micrometers, which is consistent with the observed grain sizes in Fig. 3. Therefore, with decreasing electrode spacing close to the domain size, the resistance change for $VO_2$ on hBN is expected to be more step-like, and, ultimately, to exhibit a single step across the MIT, as observed in single-crystalline $VO_2$[2].

Finally, although the actual fabrication of devices is beyond the scope of this paper, we performed a transfer of the $VO_2$/hBN stack for device applications. Figure 6a,b show optical images of the $VO_2$/hBN stack before and after the transfer process. See Methods for details of the pick-up and transfer process. By this process, the stacks were uniformly transferred from the substrate to the polymer film, as can be confirmed from the Raman spectra for $VO_2$ in Fig. 6c. The polymer film has an elastomeric property and has been previously commonly used for stretchable electronics[42]. Therefore, the $VO_2$/hBN stacks supported on the polymer could form the basis of electronic

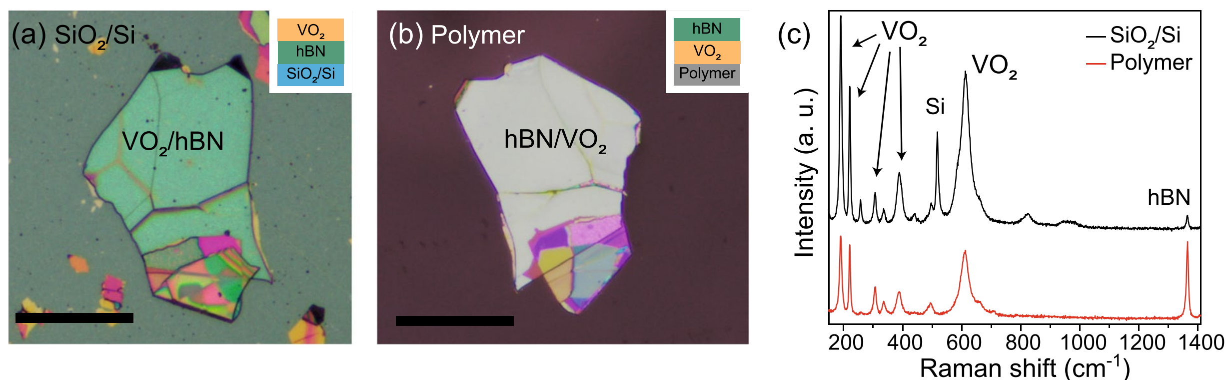


**Figure 6.** Optical images of the $VO_2$/hBN stack on (**a**) the $SiO_2$/Si substrate and (**b**) transferred onto the polymer film. The scale bars are 50 µm. The insets in (**a**,**b**) show schematic illustrations of the stacking structure. (**c**) Raman spectra for the $VO_2$/hBN stack before (black curve) and after (red curve) the transfer process. The prominent peaks due to the vibrational modes of $VO_2$ can be seen even after the transfer.

and optical switching devices with flexibility, bendability, and stretchability. To further validate the transferability of the $VO_2$/hBN stacks, we transferred the stacks from the polymer films to other substrates such as gold, glass slide and paper, where the direct growth of a high-quality $VO_2$ thin film is challenging (see Supplementary Information for optical images of $VO_2$/hBN transferred onto these substrates). The Raman spectroscopy measurements confirmed uniform crystallinity for the transferred $VO_2$, suggesting the utility of hBN as a transferrable substrate.

## Conclusion

We demonstrated growth of $VO_2$ crystals on an insulating layered material, hBN. The $VO_2$ film is polycrystalline, but the mean grain size was observed to reach up-to micrometers. The $VO_2$ thin film is grown preferentially with the (110) orientation, which is predicted by the DFT calculation to be the most energetically stable[38]. Thin films of $VO_2$ on hBN undergo a MIT at approximately 340 K, with the electrical resistance changing by nearly three orders of magnitude, showing high quality comparable to those of $VO_2$ films grown on common substrates[6–10]. Most importantly, $VO_2$ thin films could be transferred onto arbitrary surfaces with the supporting hBN; therefore, a broad spectrum of applications in electronics and photonics can be envisioned. For example, by transfer of the $VO_2$/hBN stack onto an elastomer, flexible and stretchable devices could be fabricated. Thin flakes of hBN show good insulating and dielectric properties and also show atomically flat surfaces[43]. Therefore, the $VO_2$/hBN heterostructure could form the basis of a "Mott transistor"[44], where the MIT is controlled by gating. Additionally, the $VO_2$/hBN heterostructure could behave as a reconfigurable hyperbolic metasurface[45], with great potential for applications in nanophotonic devices. Moreover, due to an inert surface with no dangling bonds, hBN is expected to have a wide degree of freedom as a substrate for oxide thin film growth.

## Methods

**Growth of $VO_2$ thin films on hBN flakes.** Thin films of $VO_2$ were grown onto hBN flakes by PLD using an argon fluoride excimer laser with a wavelength of 193 nm under an oxygen pressure of 0.95 Pa at a substrate temperature of 450 °C. The repetition rate was 2 Hz and the growth time was 5 h. A vanadium pentoxide pellet was used for the target.

**Characterization.** The Raman spectroscopy measurements were conducted using a commercial system (Raman Touch, Nanophoton) with a solid state laser operating at a wavelength of 532 nm at 300–380 K. The temperature was controlled by placing a sample onto a thermally conductive plate connected to a Peltier heating/cooling device. The grating size was 1200 lines/cm. The laser spot size was ~ 1 µm and the laser power was set to be either 0.2 or 1 mW. The AFM measurements were conducted at room temperature in the ambient with the dynamic force mode using Si cantilevers (SPA-300HV, Hitachi High-Tech Science). The HAADF-STEM measurements were performed using a JEOL JEM-ARM200F ACCELARM operated at an acceleration voltage of 200 kV. The probe semi-angle was 18 mrad. The probe current was 9 pA. The angular detection range of the HAADF detector for the scattered electrons was 50–150 mrad.

**Electrical measurements.** The stacks of $VO_2$/hBN were etched into microwires by photolithography and reactive ion etching (RIE) under a mixture of $O_2$ and sulfur hexafluoride gases. The contacting electrodes were prepared by photolithography and sputtering deposition of Cr (5 nm) and Pt (200 nm). Electrical measurements were conducted in air using a source measurement unit (2635A, Keithley) at temperatures ranging from 300 to 378 K, which was controlled by the Peltier heating/cooling system.

**Pick-up and transfer process.** To pick-up the stack of $VO_2$ and hBN, we used commercially available polymer films (PF Gel-Film, Gel-Pak)[46] treated with water vapor, which show enhanced adhesion[47]. The polymer film covered with a thin water layer was placed onto the $SiO_2$/Si substrate with the $VO_2$/hBN stacks, and, then, was slowly peeled off from the substrate. The polymer films with the stacks were placed onto the target

substrates using a transfer system (IZU-NNHA, Izumi-Tech), which was equipped with an optical microscope and micromanipulator.

## Data Availability

All data generated or analyzed during this study are included in this published article and its Supplementary Information file.

## References


1. Liu, K., Lee, S., Yang, S., Delaire, O. & Wu, J. Recent progresses on physics and applications of vanadium dioxide. *Mater. Today* **21**, 875–896 (2018).
2. Mun, B. S. *et al*. Nonpercolative metal-insulator transition in $VO_2$ single crystals. *Phys. Rev. B - Condens. Matter Mater. Phys.* **84**, 3–6 (2011).
3. Chain, E. E. Optical properties of vanadium dioxide and vanadium pentoxide thin films. *Appl. Opt.* **30**, 2782–2787 (1991).
4. Nag, J. & Haglund, R. F. Synthesis of vanadium dioxide thin films and nanoparticles. *J. Phys. Condens. Matter* **20**, 1–14 (2008).
5. Zhang, H.-T. *et al*. Wafer-scale growth of $VO_2$ thin films using a combinatorial approach. *Nat. Commun.* **6**, 8475 (2015).
6. Kim, D. H. & Kwok, H. S. Pulsed laser deposition of $VO_2$ thin films. *Appl. Phys. Lett.* **65**, 3188–3190 (1994).
7. Muraoka, Y. & Hiroi, Z. Metal–insulator transition of $VO_2$ thin films grown on $TiO_2$ (001) and (110) substrates. *Appl. Phys. Lett.* **80**, 583–585 (2002).
8. Okimura, K. & Kubo, N. Preparation of $VO_2$ films with metal-insulator transition on sapphire and silicon substrates by inductively coupled plasma-assisted sputtering. *Jpn. J. Appl. Phys.* **44**, 1150–1153 (2005).
9. Yang, Z., Ko, C. & Ramanathan, S. Metal-insulator transition characteristics of $VO_2$ thin films grown on Ge(100) single crystals. *J. Appl. Phys.* **108**, 073708 (2010).
10. Zhou, Y. & Ramanathan, S. Heteroepitaxial $VO_2$ thin films on GaN: Structure and metal-insulator transition characteristics. *J. Appl. Phys.* **112**, 074114 (2012).
11. Kim, H. *et al*. Flexible thermochromic window based on hybridized $VO_2$/graphene. *ACS Nano* **7**, 5769–5776 (2013).
12. Kim, H. *et al*. Enhanced optical response of hybridized $VO_2$/graphene films. *Nanoscale* **5**, 2632–2636 (2013).
13. Yan, J., Huang, W., Zhang, Y., Liu, X. & Tu, M. Characterization of preferred orientated vanadium dioxide film on muscovite (001) substrate. *Phys. Stat. Sol. (a)* **205**, 2409–2412 (2008).
14. Li, C.-I. *et al*. van der Waal epitaxy of flexible and transparent $VO_2$ film on muscovite. *Chem. Mater.* **28**, 3914–3919 (2016).
15. Britnell, L. *et al*. Electron tunneling through ultrathin boron nitride crystalline barriers. *Nano Lett.* **12**, 1707–1710 (2012).
16. Lee, G.-H. *et al*. Electron tunneling through atomically flat and ultrathin hexagonal boron nitride. *Appl. Phys. Lett.* **99**, 243114 (2011).
17. Watanabe, K., Taniguchi, T. & Kanda, H. Direct-bandgap properties and evidence for ultraviolet lasing of hexagonal boron nitride single crystal. *Nat. Mater.* **3**, 404–409 (2004).
18. Cassabois, G., Valvin, P. & Gil, B. Hexagonal boron nitride is an indirect bandgap semiconductor. *Nat. Photon.* **10**, 262–266 (2016).
19. Falin, A. *et al*. Mechanical properties of atomically thin boron nitride and the role of interlayer interactions. *Nat. Commun.* **8**, 15815 (2017).
20. Garcia, A. G. F. *et al*. Effective cleaning of hexagonal boron nitride for graphene devices. *Nano Lett.* **12**, 4449–4454 (2012).
21. Li, L. H., Cervenka, J., Watanabe, K., Taniguchi, T. & Chen, Y. Strong oxidation resistance of atomically thin boron nitride nanosheets. *ACS Nano* **8**, 1457–1462 (2014).
22. Taniguchi, T. & Watanabe, K. Synthesis of high-purity boron nitride single crystals under high pressure by using Ba-BN solvent. *J. Cryst. Growth* **303**, 525–529 (2007).
23. Parker, J. H. Jr., Feldman, D. W. & Ashkin, M. Raman scattering by silicon and germanium. *Phys. Rev.* **155**, 712–714 (1967).
24. Geick, R., Perry, C. & Rupprecht, G. Normal modes in hexagonal boron nitride. *Phys. Rev.* **146**, 543–547 (1966).
25. Pan, M. *et al*. Raman study of the phase transition in $VO_2$ thin films. *J. Cryst. Growth* **268**, 178–183 (2004).
26. Okimura, K. *et al*. Temperature-dependent Raman and ultraviolet photoelectron spectroscopy studies on phase transition behavior of $VO_2$ films with M1 and M2 phases. *J. Appl. Phys.* **115**, 153501 (2014).
27. Marezio, M., McWhan, D. B., Remeika, J. P. & Dernier, P. D. Structural aspects of the metal-insulator transitions in Cr-doped $VO_2$. *Phys. Rev. B* **5**, 2541–2551 (1972).
28. Strelcov, E. *et al*. Doping-based stabilization of the M2 phase in free-standing $VO_2$ nanostructures at room temperature. *Nano Lett.* **12**, 6198–6205 (2012).
29. Atkin, J. M. *et al*. Strain and temperature dependence of the insulating phases of $VO_2$ near the metal-insulator transition. *Phys. Rev. B - Condens. Matter Mater. Phys.* **85**, 020101(R) (2012).
30. Okimura, K., Watanabe, T. & Sakai, J. Stress-induced $VO_2$ films with M2 monoclinic phase stable at room temperature grown by inductively coupled plasma-assisted reactive sputtering. *J. Appl. Phys.* **111**, 073514 (2012).
31. Sun, X., Shi, J., Washington, M. A. & Lu, T.-M. Probing the interface strain in a 3D-2D van der Waals heterostructure. *Appl. Phys. Lett.* **111**, 151603 (2017).
32. Petrov, G. I., Yakovlev, V. V. & Squier, J. Raman microscopy analysis of phase transformation mechanisms in vanadium dioxide. *Appl. Phys. Lett.* **81**, 1023–1025 (2002).
33. Mendelson, M. I. Average grain size in polycrystalline ceramics. *J. Am. Ceram. Soc.* **52**, 443–446 (1969).
34. Xu, G., Jin, P., Tazawa, M. & Yoshimura, K. Thickness dependence of optical properties of $VO_2$ thin films epitaxially grown on sapphire (0001). *Appl. Surf. Sci.* **244**, 449–452 (2005).
35. Amram, D., Klinger, L., Gazit, N., Gluska, H. & Rabkin, E. Grain boundary grooving in thin films revisited: The role of interface diffusion. *Acta Mater.* **69**, 386–396 (2014).
36. Cho, Y. *et al*. Morphology of phase-separated $VO_2$ films deposited on $TiO_2$-(001) substrate. *Mater. Res. Bull.* **102**, 289–293 (2018).
37. Gu, Y., Cao, J., Wu, J. & Chen, L.-Q. Thermodynamics of strained vanadium dioxide single crystals. *J. Appl. Phys.* **108**, 083517 (2010).
38. Mellan, T. A. & Grau-Crespo, R. Density functional theory study of rutile $VO_2$ surfaces. *J. Chem. Phys.* **137**, 154706 (2012).
39. Christenson, H. K. & Thomson, N. H. The nature of the air-cleaved mica surface. *Surf. Sci. Rep.* **71**, 367–390 (2016).
40. Sharoni, A., Ramírez, J. G. & Schuller, I. K. Multiple avalanches across the metal-insulator transition of vanadium oxide nanoscaled junctions. *Phys. Rev. Lett.* **101**, 4–7 (2008).
41. Kawatani, K., Takami, H., Kanki, T. & Tanaka, H. Metal-insulator transition with multiple micro-scaled avalanches in $VO_2$ thin film on $TiO_2$(001) substrates. *Appl. Phys. Lett.* **100**, 173112 (2012).
42. Rogers, J. A., Someya, T. & Huang, Y. Materials and mechanics for stretchable electronics. *Science* **327**, 1603–1607 (2010).
43. Dean, C. R. *et al*. Boron nitride substrates for high-quality graphene electronics. *Nat. Nanotechnol.* **5**, 722–726 (2010).
44. Yang, Z., Ko, C. & Ramanathan, S. Oxide electronics utilizing ultrafast metal-insulator transitions. *Annu. Rev. Mater. Res.* **41**, 337–367 (2011).
45. Folland, T. G. *et al*. Reconfigurable infrared hyperbolic metasurfaces using phase change materials. *Nat. Commun.* **9**, 4371 (2018).
46. Castellanos-Gomez, A. *et al*. Deterministic transfer of two-dimensional materials by all-dry viscoelastic stamping. *2D Mater.* **1**, 011002 (2014).
47. Ma, X. *et al*. Capillary-force-assisted clean-stamp transfer of two-dimensional materials. *Nano Lett.* **17**, 6961–6967 (2017).

## Acknowledgements

The authors would like to thank S. Sakakihara for carrying out the RIE process. This work was partly supported by JSPS KAKENHI Grant Numbers 17K14658, 16H03871, 26248061, and 17H01054, the Yazaki Memorial Foundation for Science and Technology, the Research Program of "Five-star Alliance" in "NJRC Mater. & Dev.", and the Nanotechnology Platform Project (Nanotechnology Open Facilities in Osaka University) of the MEXT, Japan (Nos F-16-OS-0012 and F-16-OS-0016).


## Author Contributions

M.Y. and H.T. conceived the experiment. H.T. directed the project. S.G. performed the PLD growth of $VO_2$ on hBN and conducted the AFM, Raman spectroscopy, and electrical measurements. M.Y. and T.K. assisted the experiments. S.G. and M.Y. analyzed the experimental data. K.S., S.A. and Y.M. performed the STEM measurements. K.S., S.A., Y.M., S.G., M.Y. and H.T. analyzed the STEM results. S.G., M.Y. and R.N. conducted the transfer process. K.W. and T.T. synthesized the high-purity hBN crystals. M.Y. and S.G. prepared the manuscript using substantial inputs from the other authors. All the authors discussed the experimental results.

## Additional Information

**Supplementary information** accompanies this paper at https://doi.org/10.1038/s41598-019-39091-8.

**Competing Interests:** The authors declare no competing interests.

**Publisher's note:** Springer Nature remains neutral with regard to jurisdictional claims in published maps and institutional affiliations.

**Open Access** This article is licensed under a Creative Commons Attribution 4.0 International License, which permits use, sharing, adaptation, distribution and reproduction in any medium or format, as long as you give appropriate credit to the original author(s) and the source, provide a link to the Creative Commons license, and indicate if changes were made. The images or other third party material in this article are included in the article's Creative Commons license, unless indicated otherwise in a credit line to the material. If material is not included in the article's Creative Commons license and your intended use is not permitted by statutory regulation or exceeds the permitted use, you will need to obtain permission directly from the copyright holder. To view a copy of this license, visit http://creativecommons.org/licenses/by/4.0/.

© The Author(s) 2019